Influence of dynamic power dissipation on Si MRM modulation characteristics

Byung-Min Yu[1], Myungjin Shin[1], Min-Hyeong Kim[1], Lars Zimmermann[2], and Woo-Young Choi[1,*]

[1]*Department of Electrical and Electronic Engineering, Yonsei University, Seoul 120-749, South Korea*
[2]*Innovations for High Performance Microelectronics (IHP), Frankfurt (Oder) 15236, Germany*
**Corresponding author: wchoi@yonsei.ac.kr*

Received January 10, 2017; accepted March 24, 2017; posted online April 20, 2017

We experimentally observe that Si micro-ring modulator (MRM) modulation characteristics are strongly influenced by the modulation data rate and the data pattern and determine this influence is due to the temperature increase caused by dynamic power dissipation within the Si MRM device. We also quantitatively determine the amount of Si MRM resonance wavelength shift due to different modulation data rates, data patterns, and modulation voltages. Our results should be of great help for achieving reliable and optimal modulation characteristics for Si MRMs.

OCIS codes: 130.4110, 230.4110, 230.5750, 250.4110.
doi: 10.3788/COL201715.071301.

Optical interconnects are intensively investigated as a replacement for electrical interconnects, which suffer from loss for high-frequency signals and crosstalk in many demanding high-bandwidth interconnect applications[1–3]. In particular, Si photonics has emerged as a promising solution for such applications as rack-to-rack and server-to-server optical interconnects in data centers because it can provide high-bandwidth photonic components that can be integrated in a cost-effective manner using well-established Si fabrication technology[4]. Among many photonic devices that can be realized with Si photonics, the depletion-type Si micro-ring modulator (MRM) has received a great amount of research interest since it can provide high-speed modulation with a very small footprint and wavelength division multiplexing (WDM) compatibility[5].

However, its characteristics are strongly influenced by temperature, as any perturbation on the Si reflective index due to temperature variations causes a significant amount of changes in the ring resonator characterizations. There are a number of reports that investigated the influence of temperature on Si MRMs' modulation characteristics[6,7].

In this Letter, we report our experimental observation that Si MRM modulation characteristics are strongly influenced by the modulation data rate and the data pattern. We determine that this influence is due to the temperature increase caused by dynamic power dissipation within the Si MRM device. We provide measurement results with which the cause of the data-dependent Si MRM characteristics is clearly identified. Our results can be used for designing Si ring modulator structures that suffer less from dynamic power dissipation and, consequently, result in more reliable Si MRM operation and can determine the range of thermal tuning required for optimal operation of Si ring modulators for the required range of data rates.

Figure 1(a) shows the structure of the Si MRM device used for our investigation, which has been fabricated in Si photonic integrated circuit multi-project wafer (PIC MPW) provided by IHP. The ring has an 8-μm radius and a 290-nm gap between the ring and the bus waveguide. Figure 1(b) shows the cross section of the Si MRM. The device has a 220-nm thick Si waveguide above a 2-μm thick buried oxide (BOX) layer and 500-nm-wide ring and bus waveguides. The waveguide contains a P-N junction, which has a nominal peak doping concentration of 7×10^{17} cm^{-3} for the P region and 5×10^{18} cm^{-3} for the N region. Figure 1(c) shows the measured modulation frequency responses for five different values of wavelength detuning from the ring resonance wavelength. The same device was used for the Si MRM self-heating investigation reported in Ref. [8] and establishing Si MRM linear circuit models in Ref. [9].

Figure 2 shows the measurement setup. CW light from a tunable laser is coupled through the on-chip grating coupler into the device, which is either DC biased or modulated with various NRZ data signals generated by a pulse pattern generator (PPG). The optical power spectrum and the eye diagram are observed with an optical spectrum analyzer and an optical oscilloscope, respectively.

Figure 3(a) shows the measured transmission spectrum of the Si MRM biased at −2 V without any data signal. For this measurement and others whose results are shown in Figs. 3–6, the power of the input light coupled into the Si MRM device is kept at −13 dBm so that the device does not suffer from self-heating. Figure 3(b) shows the measured eye diagrams of the Si MRM modulated with nonreturn-to-zero (NRZ) data signals having four different data rates but with the same input wavelength indicated in Fig. 3(a). For this measurement, 2^{31}–1 pseudorandom bit sequence (PRBS) data having V_{mod} of 4 V_{pp} are applied to the modulator. Clearly, the modulation characteristics strongly depend on the data rate.

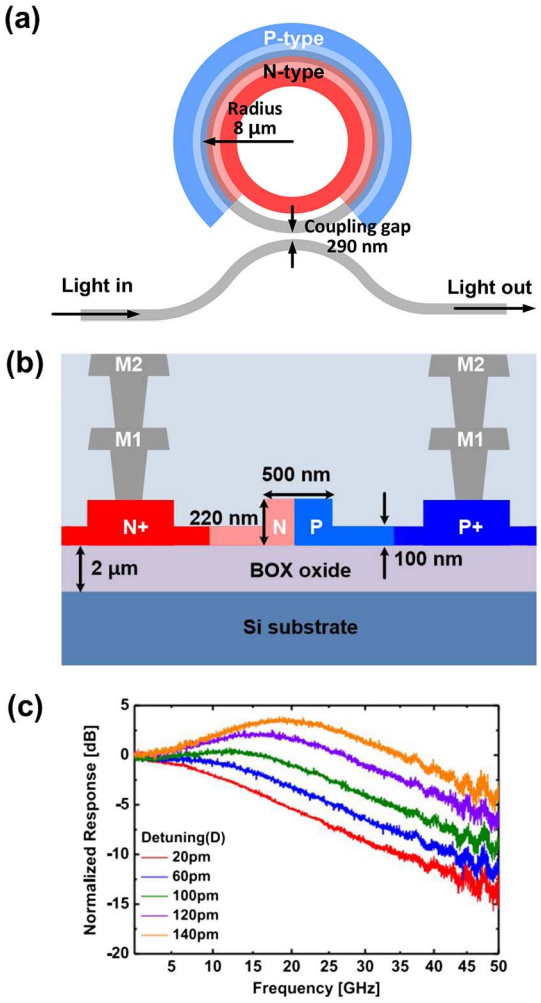

Fig. 1. (a) Structure of Si MRM, (b) cross section of Si MRM, and (c) measured electro-optic S_{21} at five different detuning values[8].

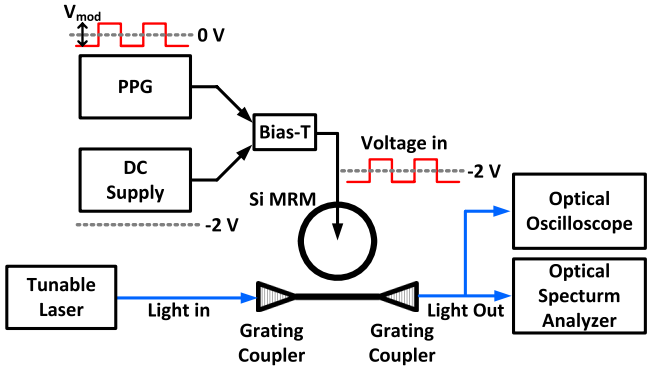

Fig. 2. Measurement setup.

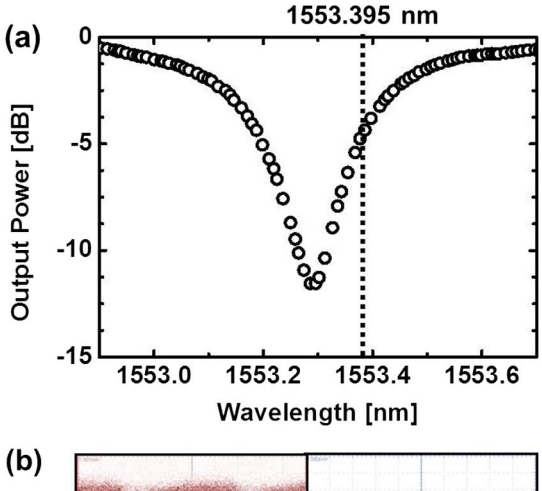

Fig. 3. (a) Narrowband transmission spectrum of Si MRM and (b) eye diagrams for various data rates at 1553.395-nm input wavelength.

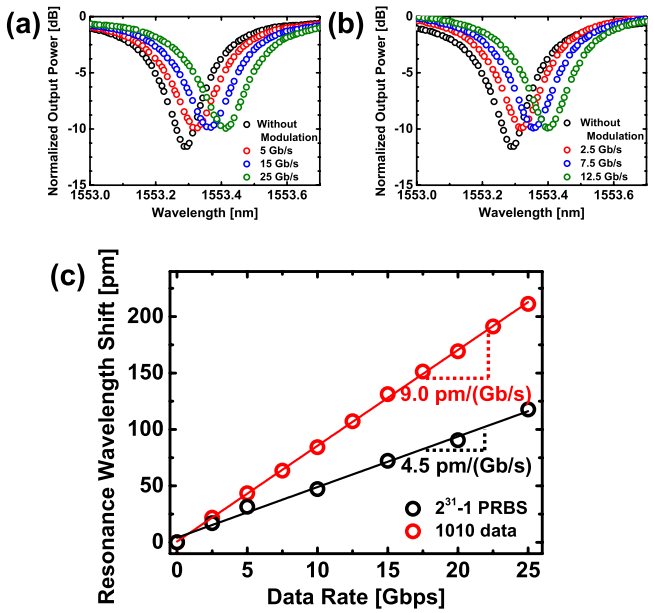

Fig. 4. Transmission spectra measured under data modulation with different data patterns: (a) PRBS 2^{31}-1 and (b) "1010" data. (c) Resonance wavelength shift dependence on data rates for two different data patterns.

In order to identify the cause of this dependency, Si MRM transmission characteristics are measured when the device is electrically modulated with different data rates and different data patterns. Figures 4(a) and 4(b) show the transmission spectra measured without any data modulation and with data modulation at three different data rates. 2^{31}–1 PRBS data are used for Fig. 4(a) and periodic 1010 data for Fig. 4(b). From these, two observations can be made. One, the transmitted power at the resonance wavelength increases with the data modulation,

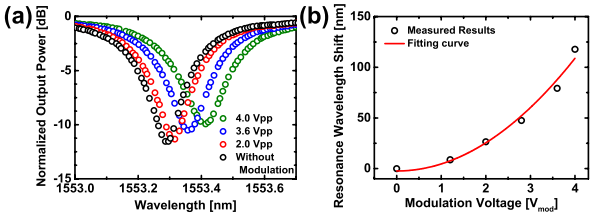

Fig. 5. (a) Transmission spectra measured under data modulation with different modulation voltages and (b) resonance wavelength shift dependence on modulation voltages.

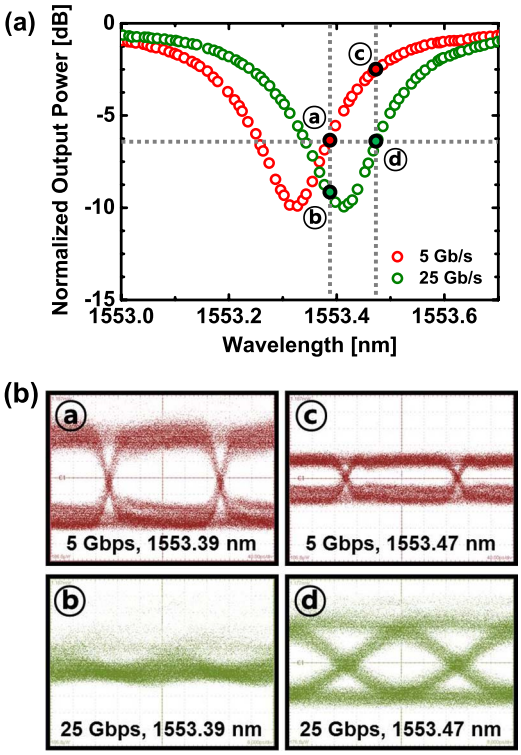

Fig. 6. (a) Transmission spectra with data modulation at 5 and 25 Gb/s and (b) eye diagrams at different conditions.

and the other, the resonance wavelength increases with the data rate. The first observation can be easily explained by the fact that modulation causes spectral broadening of the input light, which, in turn, causes the broadening of the resonance peak. For better understanding of the second observation, the resonance wavelength is plotted as a function of the data rate for two different data patterns in Fig. 4(c). A clear linear dependence is observed with a larger slope for the PRBS data than for the 1010 data.

An additional transmission spectrum measurement with data modulation is done for different V_{mod} values applied to the Si MRM. Figure 5(a) shows the resulting normalized transmission characteristics for the case of no data modulation and modulation, with 25-Gb/s $2^{31}-1$ PRBS having V_{mod} of 2.0, 3.6, and 4.0 V_{pp}. Figure 5(b) shows the dependence of the resonance wavelength shift on the modulation voltage (V_{mod}). As can be seen in the figure, the wavelength shift has a quadratic dependence on the modulation voltage applied to the Si MRM.

The above observations can be explained by the fact that electrically, the Si MRM is a capacitive load in which AC currents are produced whenever the applied voltage switches. These AC currents induce ohmic heating in the series resistor within the Si MRM or the dynamic power dissipation. With this, the device temperature rises, causing the increase in the refractive index of Si, resulting in the red-shift of the resonance wavelength.

It is well known that the dynamic power dissipation of a capacitive load is given as[10]

$$P = \alpha \times C \times V^2 \times f, \tag{1}$$

where α is the data transition rate, C is the load capacitance, V is the modulation voltage applied, and f is the data rate. For the PRBS data, $\alpha = 0.25$, and for the 1010 data, $\alpha = 0.5$. Since the resonance wavelength shift is proportional to the temperature increase, which is proportional to the dynamic power dissipation, the above equation clearly explains why the resonance wavelength shift is linearly proportional to the data rate, why the 1010 data has twice as large a slope as the PRBS data, and why the resonance wavelength shift has a quadratic dependence on the modulation voltage.

An Si MRM can be electrically modeled with a series resistor and junction capacitance, as shown in Fig. 7. The numerical values of these components in our Si MRM can be determined from the electrical S parameter measurement as C_j of 14.5 fF and R_s of 280 Ω[9]. Since the dynamic power is dissipated both in R_s and R_{out} in Fig. 7, where R_{out} represents the 50-Ω output impedance of the PPG used for measurement, the dynamic power dissipated inside the Si MRM can be determined by multiplying $R_s/(R_s + R_{\mathrm{out}})$ with Eq. (1). With this, for 25-Gb/s modulation with 4-V_{pp} 2^{31}–1 PRBS, the dissipated dynamic power inside our Si MRM is 1.23 mW. Clearly, this dynamic power dissipation can be reduced if the Si MRM is realized with reduced C_j and/or R_s. This amount of dynamic power dissipation causes the resonance wavelength shift of 112 pm, as can be seen in Fig. 4(c), which, with the known temperature dependence of the Si refractive index[11], corresponds to about a 1.9 K increase in the temperature.

The above discussions give a clear explanation for the different eye diagrams observed for the different data rates shown in Fig. 3. The Si MRM has different transmission

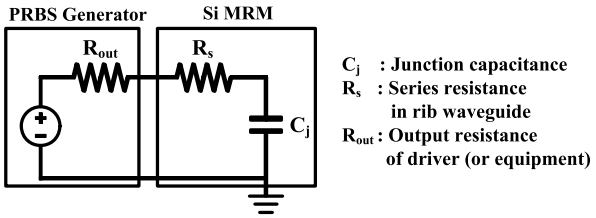

Fig. 7. Electrical model of Si MRM.

characteristics with different resonance wavelengths for different modulation data rates. Consequently, the amount of detuning, or separation between the input wavelength and the resonance wavelength, is different for different data rates. The Si MRM modulation frequency responses greatly depend on the amount of detuning, as shown in Fig. 1(c), resulting in different eye diagrams[12].

Figure 6 demonstrates that optimal eye diagrams can be obtained for different data rates if the input light wavelength is shifted by the correct amount or a temperature control of the Si MRM is implemented so that it provides the same transmitted output power even if modulation data rates are different. These results should be of great help for implementing temperature stabilization circuits for reliable operation of Si MRMs[7,13].

In conclusion, we investigate the influence of dynamic power dissipation on Si MRM modulation characteristics. We clearly demonstrate that device temperature increase due to dynamic power dissipation, which depends on the data rate, data pattern, device capacitance, and modulation voltage, strongly influences Si modulation characteristics.

This work was supported by the National Research Foundation of Korea grant funded by the Korean Ministry of Science, ICT and Future Planning (No. 2015R1A2A2A01007772) and the Materials and Parts Technology R&D Program funded by the Korean Ministry of Trade, Industry & Energy (Project No. 10065666).

References

1. D. A. B. Miller, IEEE J. Sel. Top. Quantum Electron. **6**, 1312 (2000).
2. J. D. Meindl, J. A. Davis, P. Zarkesh-Ha, C. S. Patel, K. P. Martin, and P. A. Kohl, IBM J. Res. Dev. **46**, 245 (2002).
3. O. Kibar, D. A. Van Blerkom, C. Fan, and S. C. Esener, J. Lightwave Technol. **17**, 546 (1999).
4. R. Soref, IEEE J. Sel. Top. Quantum Electron. **12**, 1678 (2006).
5. T. Baba, S. Akiyama, M. Imai, N. Hirayama, H. Takahashi, Y. Noguchi, T. Horikawa, and T. Usuki, Opt. Express **21**, 11869 (2013).
6. S. Saeedi and A. Emami, Opt. Express **23**, 21875 (2015).
7. K. Padmaraju, D. F. Logan, X. Zhu, J. J. Ackert, A. P. Knights, and K. Bergman, Opt. Express **21**, 14342 (2013).
8. M. Shin, Y. Ban, B.-M. Yu, J. Rhim, L. Zimmermann, and W.-Y. Choi, IEEE J. Sel. Top. Quantum Electron. **22**, 3400207 (2016).
9. M. Shin, Y. Ban, B.-M. Yu, M.-H. Kim, J. Rhim, L. Zimmermann, and W.-Y. Choi, IEEE Trans. Electron Devices **64**, 1140 (2017).
10. J. M. Rabaey, A. P. Chandrakasan, and B. Nikolic, *Digital Integrated Circuit*, 2nd ed. (Pearson, 2003).
11. M. S. Nawrocka, T. Liu, X. Wang, and R. R. Panepucci, Appl. Phys. Lett. **89**, 071110 (2006).
12. J. Rhim, B.-M. Yu, J.-M. Lee, S.-H. Cho, and W.-Y. Choi, in *Optical Interconnects Conference* (2016).
13. C. Li, R. Bai, A. Shafik, E. Z. Tabasy, B. Wang, G. Tang, C. Ma, C.-H. Chen, Z. Peng, M. Fiorentino, R. G. Beausoleil, P. Chiang, and S. Palermo, IEEE J. Solid-State Circuits **49**, 1419 (2014).